Published OnlineFirst March 13, 2018; DOI: 10.1158/1078-0432.CCR-17-3081

Translational Cancer Mechanisms and Therapy

Clinical Cancer Research

RIP1–HAT1–SIRT Complex Identification and Targeting in Treatment and Prevention of Cancer

Vincenzo Carafa[1], Angela Nebbioso[1], Francesca Cuomo[1], Dante Rotili[2], Gilda Cobellis[1], Paola Bontempo[1], Alfonso Baldi[3], Enrico P. Spugnini[4], Gennaro Citro[5], Angela Chambery[3], Rosita Russo[3], Menotti Ruvo[6], Paolo Ciana[7], Luca Maravigna[7], Jani Shaik[8], Enrico Radaelli[9,10], Pasquale De Antonellis[11], Domenico Tarantino[2], Adele Pirolli[2], Rino Ragno[2], Massimo Zollo[11,12], Hendrik G. Stunnenberg[8], Antonello Mai[2,13], and Lucia Altucci[1]

Abstract

Purpose: Alteration in cell death is a hallmark of cancer. A functional role regulating survival, apoptosis, and necroptosis has been attributed to RIP1/3 complexes.

Experimental Design: We have investigated the role of RIP1 and the effects of MC2494 in cell death induction, using different methods as flow cytometry, transcriptome analysis, immunoprecipitation, enzymatic assays, transfections, mutagenesis, and *in vivo* studies with different mice models.

Results: Here, we show that RIP1 is highly expressed in cancer, and we define a novel RIP1/3–SIRT1/2–HAT1/4 complex. Mass spectrometry identified five acetylations in the kinase and death domain of RIP1. The novel characterized pan-SIRT inhibitor, MC2494, increases RIP1 acetylation at two additional sites in the death domain. Mutagenesis of the acetylated lysine decreases RIP1-dependent cell death, suggesting a role for acetylation of the RIP1 complex in cell death modulation. Accordingly, MC2494 displays tumor-selective potential *in vitro*, in leukemic blasts *ex vivo*, and *in vivo* in both xenograft and allograft cancer models. Mechanistically, MC2494 induces bona fide tumor-restricted acetylated RIP1/caspase-8–mediated apoptosis. Excitingly, MC2494 displays tumor-preventive activity by blocking 7,12-dimethylbenz(α)anthracene–induced mammary gland hyperproliferation *in vivo*.

Conclusions: These preventive features might prove useful in patients who may benefit from a recurrence-preventive approach with low toxicity during follow-up phases and in cases of established cancer predisposition. Thus, targeting the newly identified RIP1 complex may represent an attractive novel paradigm in cancer treatment and prevention. *Clin Cancer Res; 24(12); 2886–900. ©2018 AACR.*

Introduction

Cell death is a normal process responsible of tissue homeostasis. Different pathways of cell death have been described (1) and recently classified (2, 3). Both the classical apoptosis, autophagy, and necroptosis [a new form of programmed cell death (PCD); ref. 4] have been causally connected to cancer. The RIP1 kinase has been reported displaying a functional role in either regulation of survival or apoptosis and necroptosis (5) and is a key regulator of many signaling pathways such as inflammation (6), oxidative stress, plasma membrane permeabilization, and cytosolic ATP reduction (7). RIP1, initially identified as a Fas-interacting protein (8, 9), is also named "a death domain kinase", having a 112-amino acid death domain (DD) at its C-terminus. RIP1 is the founding member of the RIP family (10). RIP1 kinase activity is responsible for RIP3 phosphorylation (11), and subsequently, for MLKL phosphorylation and trimerization, which is necessary to activate the necroptotic death pathway (12, 13). The fact that other RIP family members do not compensate for RIP1 deficiency suggests a unique role for RIP1 (10, 14). The central deregulation of cell death in tumorigenesis has become clear, yet, very little is known of RIP1 and cancer. RIP1 and RIP3, as well as necroptosis, are deregulated in many types of cancers, thus

[1]Dipartimento di Medicina di Precisione, Università degli Studi della Campania "Luigi Vanvitelli", Napoli, Italy. [2]Dipartimento di Chimica e Tecnologie del Farmaco, "Sapienza" Università di Roma, Roma, Italy. [3]Dipartimento di Scienze e Tecnologie Ambientali Biologiche e Farmaceutiche, Università della Campania Luigi Vanvitelli, Caserta, Italy. [4]Biopulse s.r.l., Napoli, Italy. [5]SAFU Department, Regina Elena Cancer Institute, Rome, Italy. [6]Istituto di Biostrutture e Bioimmagini, CNR, and CIRPeB, Napoli, Italy. [7]Center of Excellence on Neurodegenerative Diseases and Department of Pharmacological Sciences, Università di Milano, Milano, Italy. [8]Department of Molecular Biology, Radboud University, Nijmegen, the Netherlands. [9]Mouse and Animal Pathology Lab, Fondazione Filarete, Milano, Italy. [10]Department of Pathobiology, School of Veterinary Medicine, University of Pennsylvania, Philadelphia, Pennsylvania. [11]CEINGE, Naples, Italy. [12]Dipartimento di Biochimica e Biotecnologie Mediche, Università Federico II, Napoli, Italy. [13]Pasteur-Fondazione Cenci Bolognetti, Sapienza Università di Roma, Roma, Italy.

Note: Supplementary data for this article are available at Clinical Cancer Research Online (http://clincancerres.aacrjournals.org/).

Corresponding Author: Lucia Altucci, Università degli Studi della Campania 'L. Vanvitelli', Vico L. De Crecchio 7, 80138 Napoli, Italy. Phone: 3908-1566-7569; Fax: 390-8145-0169; E-mail: lucia.altucci@unicampania.it

doi: 10.1158/1078-0432.CCR-17-3081

Published OnlineFirst March 13, 2018; DOI: 10.1158/1078-0432.CCR-17-3081

Translational Relevance

It is becoming increasingly clear that cancer is not only a genetic but also an epigenetic disease. Here, we identified a novel RIP1–SIRT/HAT1 complex controlling survival and death via regulation of RIP1 acetylation. Notwithstanding the increasing interest for sirtuins modulation in tumorigenesis, very little known is on their involvement in programmed cell death programs. A major goal of epi-drug development is to increase the therapeutic index and limit development of resistance. One attractive option is to combine anticancer effects with drugs able to prevent neoplasia. Here, we have developed and report on a novel pan-SIRT inhibitor that alters HAT1/SIRT equilibrium in the RIP1 complex, showing bona fide anticancer-selective and cancer-preventive activities *in vitro*, *ex vivo*, and *in vivo*. Our work expands the current views in the drug discovery and might prove useful in patients who may benefit from a recurrence-preventive approach with low toxicity during follow-up phases and in cases of established cancer predisposition.

presenting a potential therapeutic targets in treatment of cancers resistant to chemotherapeutic agents or to apoptosis inducers (15, 16). Here, we show that RIP1 is highly expressed in cancer, and we define a novel RIP1/3–SIRT1/2–HAT1/4 complex in which RIP1 is subject to regulation by acetylation. Excitingly, mutation of the acetylated lysine decreases RIP1-dependent cell death, suggesting a role for acetylation of the RIP1 complex in cell death deregulation and function. Increasing RIP1 acetylation with a novel multiacting SIRT inhibitor, MC2494, displays tumor-selective therapeutic potential *in vitro, ex vivo,* and *in vivo* inducing tumor-restricted apoptosis. Extraordinarily, MC2494 shows tumor-preventive activity *in vivo*. Thus, targeting the newly identified RIP1 complex and its acetylation may represent a feasible and attractive novel paradigm for therapeutic purposes in cancer treatment and prevention.

Materials and Methods

Cell lines, primary cells, and ligands

U937, NB4, HL-60, K562, U266, JURKAT, MCF7, MDA-MB231, LnCap, NIH3T3, and HCT116 cells were purchased from DSMZ. MCF10A was purchased from the ATCC. HEK293FT and HACAT cells were ordered from Thermo Fisher Scientific. EPN, hMSC, and primary normal amniocytes cells were obtained from University of Campania Luigi Vanvitelli, Italy. All cell lines and primary cells were grown following standard protocols. A more detailed description is reported in Supplementary Material and Methods. Mycoplasma contamination was regularly examined using a EZ-PCR Mycoplasma kit (Biological Industries), prior to freezing working stabs. All cell lines were tested and authenticated. Cells were used for experiments within 10 to 20 passages and then discarded. AGK2 (Sigma) and MC2494 (and derivatives) were dissolved in DMSO and used at 5×10^{-5} mol/L. MC2494 was synthetized by University Sapienza, Rome, Italy. For MC2494 synthesis details, see Supplementary Notes. EX527 (Alexis) was dissolved in DMSO (Sigma) and used at 5×10^{-6} mol/L, unless otherwise specified. Staurosporine (Alexis) was dissolved in DMSO and used at 2×10^{-6} mol/L. Suramin (Bio Mol) was used at 5×10^{-5} mol/L.

Antibodies

H3K9-14ac, H3K9ac, H3K56ac, and RIP1 were from Diagenode and BD. H4ac and p53ac were from Upstate. H3, Acetyllysine, H4 H2A.X (phS139), CPS1, MLYCD, SIRT1, SIRT2, PCAF, and KAT1/HAT1 were from Abcam. ATM (phS1981) and ATR were from R&D. Acetyl-tubulin was from Sigma. ERK1/2, IAP, FLIP-L, PARP, and RIP3 were from Santa Cruz Biotechnology. Bax, t-Bid, caspase-3, caspase-8, CYLD, IKKγ, FADD, FAS, and BCL2 were from Cell Signaling Technology. HAT4 was from myBiosurce.

Morphologic analysis

For U937, MCF7, and MDA-MB-231 cancer cell lines, morphologic analysis was performed, using bright field light microscopy (20X).

Reagents

Z-VAD, Z-IETD, and Z-LEHD (R&D) were used at 50 μmol/L. N-acetyl-cysteine (NAC) and Nec-1 (Sigma) were used at 50 and 100 μmol/L, respectively. Note that 1 μg of RIP1 and $RIP^{(K596/599R)}$ were transfected. H_2O_2 and PIETC (Sigma) were used at 1 mmol/L and 10 μmol/L, respectively. C646 (Sigma) was used at 50 μmol/L.

Cell vitality, cell cycle, differentiation, death, and apoptosis

To study cell vitality, experiments were performed in triplicate. Cells were diluted 1:1 in Trypan blue (Sigma) and counted. Cell cycle and differentiation analysis was performed in triplicate as reported previously (17). Apoptosis was measured by caspase-3–7, 8, and 9 (R&D) and quantified by FACS (BD). Apoptosis was measured as pre-G1 DNA fragmentation or by Annexin V detection as in ref. (17). Apoptosis versus necrosis was measured using an apoptosis/necrosis kit as suggested by the supplier (Enzo life sciences).

SIRTs, HDACs, and PCAF assays

SIRT1, 2, and 3 assay experiments were performed as suggested by the supplier (BioMol). Moreover, for SIRT1, additional assays were performed: (i) HRTF assay; (ii) BioMol assay with a different excitation/emission range; (iii) SIRTainty assay (Millipore). SIRT3 and 6 assays were performed *in vitro* following the supplier's instructions (ENZO life and Cayman, respectively). To evaluate the action of MC2494 on SIRT4 and 5, we IPed CPS1 and MLYCD (reported as substrates for SIRT4 and SIRT5, respectively), and they used in a radiolabelling assay. Finally, both histone deacetylase (HDAC) and PCAF radioactive assays were performed according to supplier's instructions (Upstate). A detailed description of *in vitro* assays is reported in Supplementary Material and Methods.

Proliferation and migration analysis in real time

Proliferation and migration analyses were evaluated in MDA-MB231 cells and performed according to the supplier instruction (xCELLigence; Roche). A detailed description is in Supplementary Material and Methods.

RNA, RT-PCR, and chromatin immunoprecipitation

Total RNA was extracted with Trizol (Invitrogen) and converted into cDNA using VILO (Invitrogen). RNA extraction and RT-PCR are detailed in the Supplementary Methods. Chromatin

Published OnlineFirst March 13, 2018; DOI: 10.1158/1078-0432.CCR-17-3081

immunoprecipitation (ChIP) was carried out as previously reported (18) using H3K9-14ac. More details are in Supplementary Material and Methods.

Protein extraction

After PBS wash, cell pellets were suspended in lysis buffer (50 mmol/L Tris-HCl, pH 7.4, 150 mmol/L NaCl, 1% NP40,

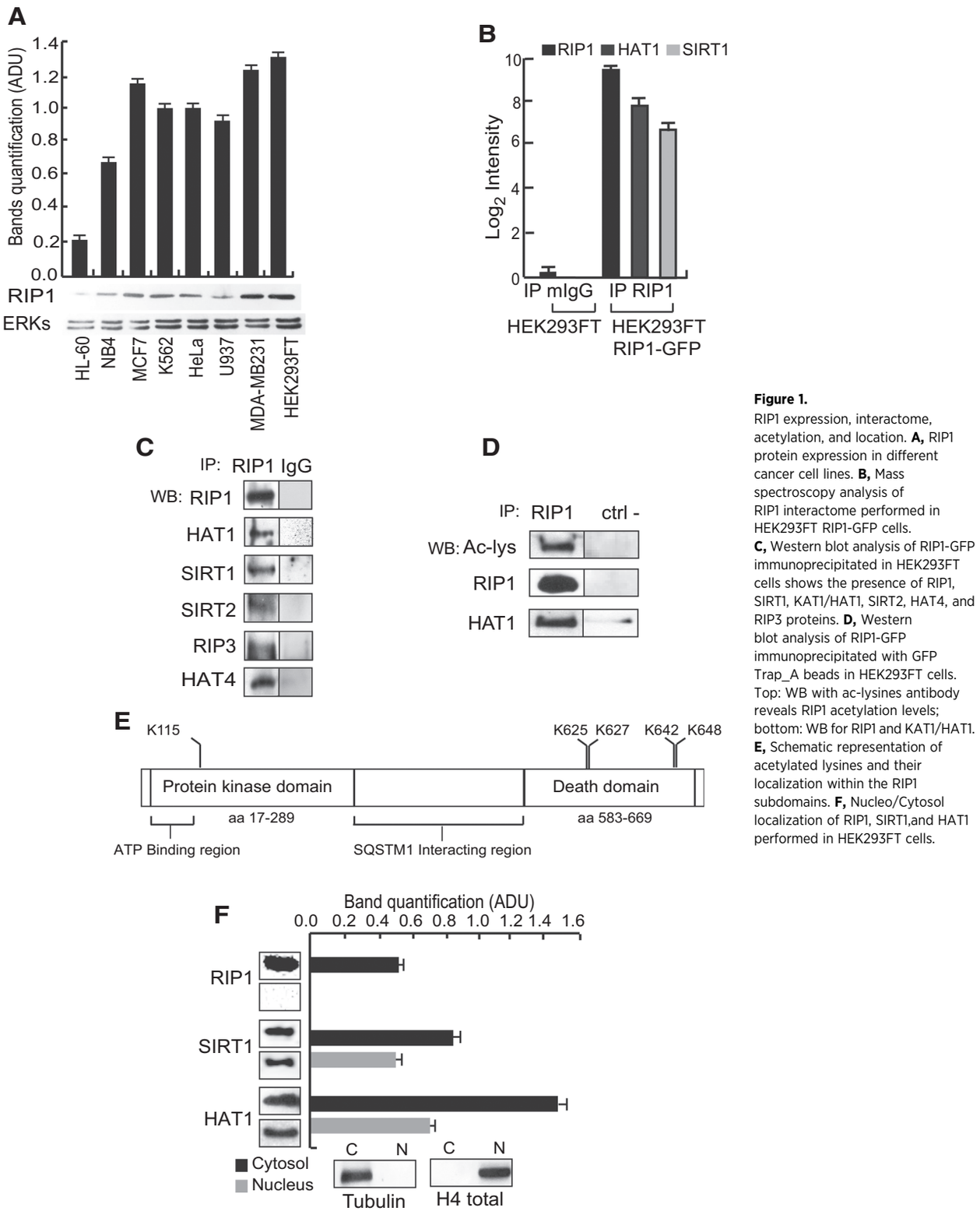

Figure 1.

RIP1 expression, interactome, acetylation, and location. **A,** RIP1 protein expression in different cancer cell lines. **B,** Mass spectroscopy analysis of RIP1 interactome performed in HEK293FT RIP1-GFP cells. **C,** Western blot analysis of RIP1-GFP immunoprecipitated in HEK293FT cells shows the presence of RIP1, SIRT1, KAT1/HAT1, SIRT2, HAT4, and RIP3 proteins. **D,** Western blot analysis of RIP1-GFP immunoprecipitated with GFP Trap_A beads in HEK293FT cells. Top: WB with ac-lysines antibody reveals RIP1 acetylation levels; bottom: WB for RIP1 and KAT1/HAT1. **E,** Schematic representation of acetylated lysines and their localization within the RIP1 subdomains. **F,** Nucleo/Cytosol localization of RIP1, SIRT1,and HAT1 performed in HEK293FT cells.

Published OnlineFirst March 13, 2018; DOI: 10.1158/1078-0432.CCR-17-3081

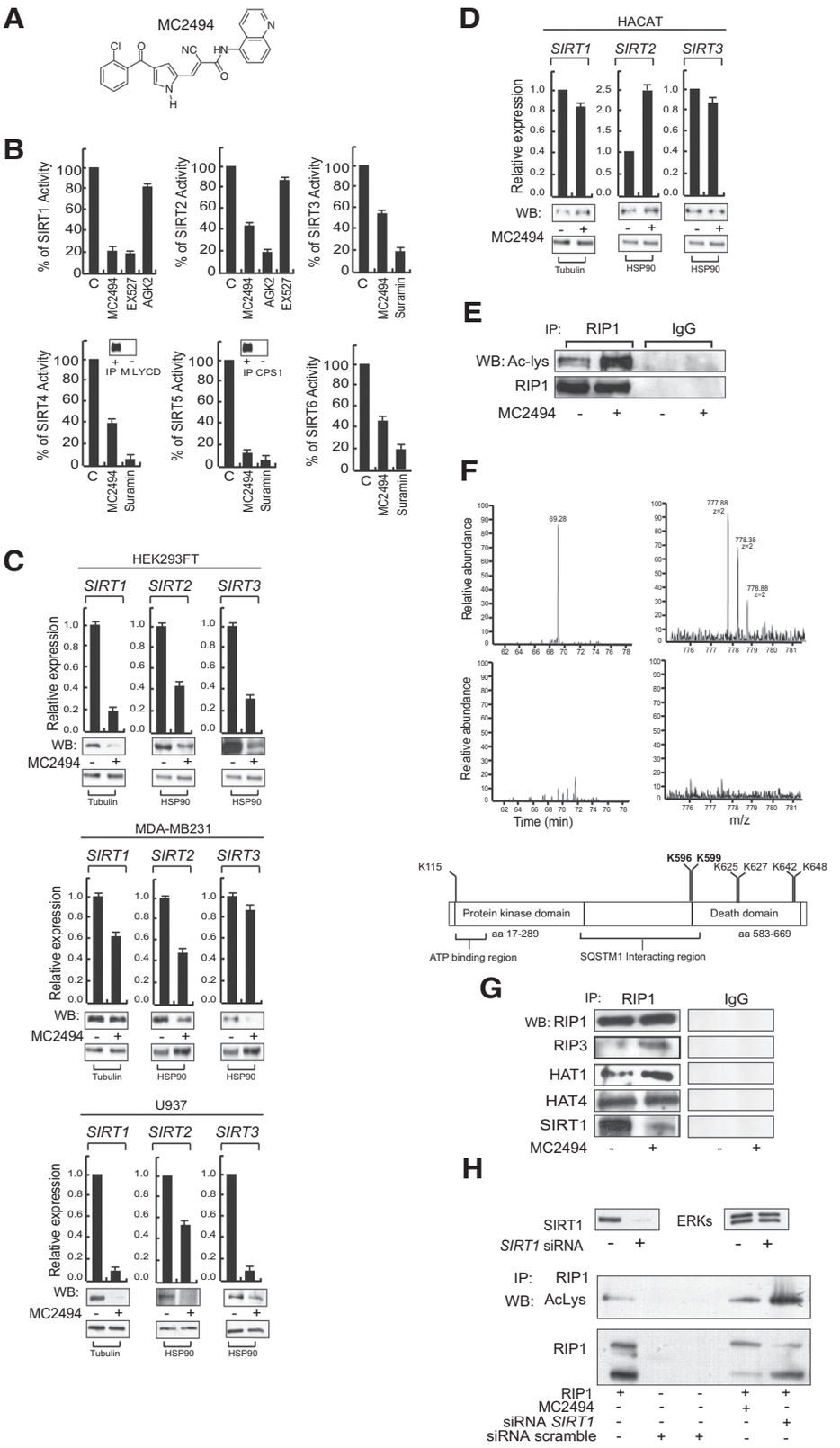

Figure 2.

The novel pan-SIRT inhibitor MC2494 affects RIP1 acetylation. **A,** Structure of MC2494. **B,** *In vitro* inhibition of SIRT1/2/3/4/5/6 by MC2494. Enzymatic assays carried out with MC2494 (50 μmol/L), Suramin (100 μmol/L), EX527 (5 μmol/L), and AGK2 (50 μmol/L) were used as controls. **C,** mRNA evaluation of *SIRT1, SIRT2*, and *SIRT3* in HEK293FT, MDA-MB231, and U937 cancer cells. **D,** mRNA evaluation of *SIRT1, SIRT2*, and *SIRT3* in HACAT "normal" cells. **E,** Western blot analysis of RIP1-GFP immunoprecipitated in HEK293FT. Top: WB with ac-lysines antibody reveals a strong increase of RIP1 acetylation levels after MC2494 treatment; Lower: WB for RIP1. **F,** Schematic representation of the acetylated lysines upon MC2494 and their localization within the RIP1 subdomains. Extracted ion chromatogram corresponding to the monoacetylated RIP1 peptides. **G,** Molecular complex analysis after MC2494 treatment. Western blot analysis of RIP1-GFP immunoprecipitates in HEK293FT cells confirms the presence of SIRT1, HAT1, RIP1, HAT4, and RIP3 proteins. After MC2494 treatment, a reduction of SIRT1 and a slight increase of HAT1 are observed. **H,** Evaluation of acetyl RIP1 in *SIRT1* loss-of-function condition. Graph showed the mean of three independent experiments with error bars indicating SD.

Published OnlineFirst March 13, 2018; DOI: 10.1158/1078-0432.CCR-17-3081

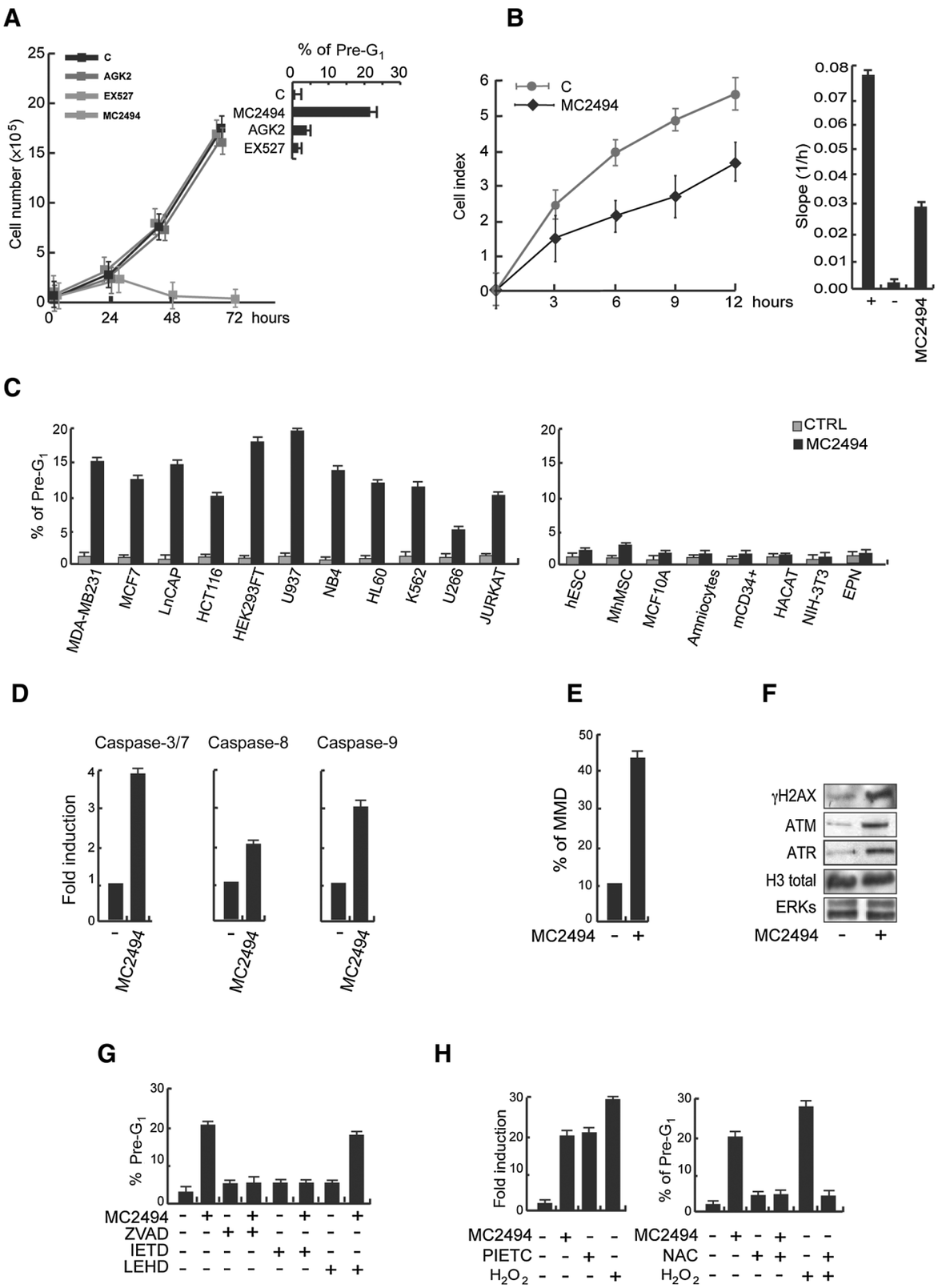

Published OnlineFirst March 13, 2018; DOI: 10.1158/1078-0432.CCR-17-3081

10 mmol/L NaF, 1 mmol/L PMSF, and protease inhibitor cocktail). The lysis reaction was carried out for 15 minutes at 4°C. Finally, the samples were centrifuged at 13,000 rpm for 30 minutes at 4°C and protein concentration quantified by Bradford assay (Bio-Rad).

Histone extraction

After stimulation with the indicated compounds, cells were collected and washed 2 times with PBS. Pellets were resuspended in triton extraction buffer [TEB; PBS containing 0.5% Triton X 100 (v/v), 2 mmol/L PMSF, 0.02% (w/v) NaN3], and the lysis procedure was performed for 10 minutes at 4°C. The samples were centrifuged at 2,000 rpm for 10 minutes at 4°C and pellets washed in TEB (half volume). Samples were then resuspended in 0.2 N HCl, and acid histone extraction was carried out overnight at 4°C. The next day the supernatant was recovered and protein concentration quantified by Bradford assay (Bio-Rad).

Nucleus/cytosol extraction

Pellets were resuspended in 2 to 2.5 volumes of NP-40 Buffer (10 mmol/L Tris-HCl, pH 7.0, 10 mmol/L NaCl, 3 mmol/L MgCl2, 30 mmol/L Sucrose, 0.5 % NP-40) and incubated for 10' on a rotating platform at 4°C. After centrifugation at 1,000 rpm for 10 minutes at 4°C, the supernatants were transfer in a new tube (cytosolic fraction). Pellets (nuclei) were suspended in 2 mL of NP-40 buffer and centrifuged at 3,000 rpm for 10 minutes. The supernatants were removed, and the pellet of nuclei was washed in Lysis Buffer (20 mmol/L Tris-HCl, pH 8, 137 mmol/L NaCl, 10% glycerol, 1% NP-40, 2 mmol/L EDTA) for 10 minutes in ice. The suspension was sonicated (4 × 30 "on/30" off high power) and centrifugated. The surnatant (nuclear proteins) was transferred in a new tube and stored at −20°C.

Western blot

Note that 50 μg of proteins were loaded on 10% to 15% polyacrylamide gels. Histone extract (5–10 μg) was loaded on 15% polyacrylamide gel. The nitrocellulose filters were stained with Ponceau red (Sigma) as additional control for equal loading. The antibodies used are listed in Supplementary Material and Methods.

Immunoprecipitation assay

MDA-MB-231 and HEK293FT cells were lysed in NP-40 (0.5%), Tris-HCl pH 8.0 (20 mmol/L), NaCl (150 mmol/L), PMSF (1 mmol/L), 10% glycerol, EDTA (1 mmol/L), and 1X protease inhibitor mix (Sigma) for 20' on ice. Cell debris was removed, and the protein-soluble fraction was incubated with antibody overnight at 4°C. The immune complexes were immunoprecipitated with Sepharose-protein A/G Plus (Santa Cruz Biotechnology) or with GFP-TRAP_A beads (Cromotech) for 2 hours at 4°C. Proteins were then eluted, resuspended, and analyzed by Western blot.

CETSA assay

HEK293FT cells were harvested and washed with PBS after treatment with MC2494 (50 μmol/L) and an equal amount of DMSO, as control, for 1 hour. The respective samples were suspended in PBS (1.5 mL), divided into aliquots (100 μL), and heated at different temperatures (25°C–37°C–44°C–53°C–57°C) for 3 minutes by Thermo Mixer (Eppendorf), followed by cooling for 3 minutes at 4°C. After incubation, lysis buffer (100 μL) was added to the samples and incubated for 15 minutes. The samples were then centrifuged at 13,000 rpm for 30 minutes at 4°C, the supernatant was removed, and protein concentration was determined using a Bradford assay (Bio-Rad). Of the total protein extract, 20 μg was loaded on 10% SDS-PAGE, and Western blot analysis was performed. The antibodies used were SIRT1, SIRT2, and SIRT3 (Abcam).

Transfections

RIP1-GFP and RIP-GFP$^{(K596/599R)}$ were transfected in HEK293FT cells with Lipofectamine 2000 (Invitrogen). TRAIL promoter mutants were used as previously described (17).

RNA interference

To silence *RIP1* and caspase-8 were used specific predesigned siRNA for *RIP1* (SI00288092) and *CASP8* (SI02661946) purchased from Qiagen. U937 cells were transfected with Nucleofector Technology, and siRNA was used at 1 μmol/L. To silence *SIRT1* gene expression, HEK293 cells were transfected with a specific *SIRT1* siRNA directed against human *SIRT1* (On-Target plus SMART pool), which was purchased from Dharmacon, and with a specific predesigned siRNA for *SIRT1* purchased from Ambion. A scrambled siRNA was used as a control. Cells were transfected with the indicated siRNAs at 50 nmol/L of concentration, using DharmaFECT1 Transfection reagent (Dharmacon).

Allograft experiments

All animal procedures were conducted according to national and international guidelines. The breast cancer 4T1–Luc model was a gift from Dr. P. Steeg (NIH, Bethesda). Approval was obtained from the Institutional Animal Care and Ethical Committee at CEINGE and "Federico II" University of Naples (Protocol #29, 01/09/2009), and the Italian Ministry of Health, Dipartimento Sanità Pubblica Veterinaria D.L. 116/92, confirming that all of the experiments conform to the relevant regulatory standards. A detailed description of procedures is in Supplementary Material and Methods.

Figure 3.

MC2494 affects proliferation and induces caspase-8–dependent apoptosis. **A,** Proliferation curve in U937 cells in the presence of the indicated compounds and analysis of cell death as evaluation of pre-G_1 phase. MC2494 and AGK2 were used at 50 μmol/L, and EX527 at 5 μmol/L. **B,** Left: MDA-MB 231 cell growth following MC2494, monitored in real time. Right: Migration rate measure as slope (1/h) monitored within the 24 hours from the indicated treatments. MC2494 was used at 50 μmol/L. **C,** Induction of pre-G_1 phase upon MC2494 treatment in cancer and normal cell lines. **D** and **E,** FACS analysis of caspase-8, -9, and -3/7 activation and MMD. The experiments were carried out in U937 cells upon treatment with MC2494 (50 μmol/L). **F,** Western blot analysis of DNA damage evaluation performed in U937 cells upon treatment with MC2494 (50 μmol/L). **G,** Apoptosis induced by MC2494 (50 μmol/L and 24 hours) in U937 cells is selectively blocked by pan- and caspase-8 inhibitors (Z-VAD and IETD), but not by caspase-9 (LEHD). **H,** ROS production following MC2494 (50 μmol/L), PIETC (10 μmol/L), and H_2O_2 (1 mmol/L) for 24 hours, and MC2494-mediated apoptosis was blocked by NAC (50 μmol/L). Curves and graph presented showed the mean of at least three different experiments with error bars indicating standard deviation.

Published OnlineFirst March 13, 2018; DOI: 10.1158/1078-0432.CCR-17-3081

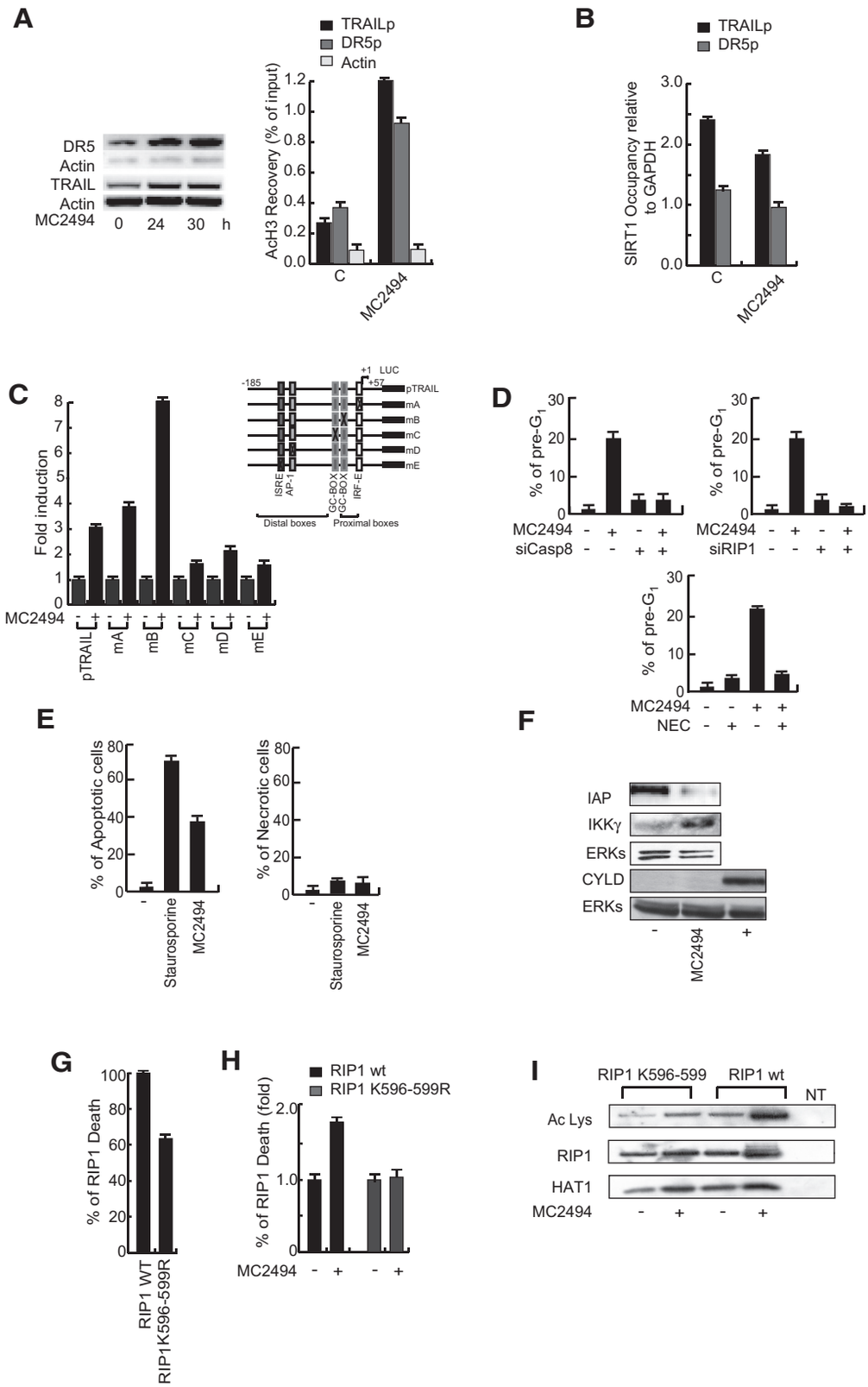

Published OnlineFirst March 13, 2018; DOI: 10.1158/1078-0432.CCR-17-3081

Cancer prevention and mito-mice

MC2494 was dissolved in DMSO and diluted 1:5 in vehicle (corn oil). 7,12-dimethylbenz(α)anthracene (DMBA; Sigma) was dissolved in acetone (8 mmol/L). Eight female MITO-Luc mice (repTOP mitoIRE; Italy; ref. 19) of 2 months of age were housed in plastic cages and fed *ad libitum* with a standard diet (4RF21 standard diet; Mucedola). Room temperature was within 22 to 25°C and humidity of 50% ± 10%. Animals were divided into two groups and s.c. treated with 50 mg/kg MC2494 or placebo (corn oil) every day at 02.00 PM for 9 days. At day 6, mice were subjected to a single s.c. intraglandular injection of DMBA (left) or vehicle (right gland); at day 9, after the last *in vivo* imaging acquisition, mice were sacrificed, mammary glands explanted for *ex vivo* imaging and fixed for analysis. A detailed description is in Supplementary Material and Methods. Imaging *in vivo* procedure was as in refs. (20, 21) and is detailed in Supplementary Material and Methods.

Xenograft experiments and pulse generator *in vivo*

All procedures involving animals and their care were conducted in conformity with institutional guidelines, which are in compliance with national (D.L. No. 116, G.U., Suppl. 40, Feb. 18, 1992; Circolare No. 8, G.U., July 1994) and international (EEC Council Directive 86/609, O.J. L 358. 1, December 12, 1987; Guide for the Care and Use of Laboratory Animals, United States National Research Council, 1996) laws. A detailed description of procedures and histology, immunohistochemistry, and TUNEL assay *in vivo* is given in Supplementary Material and Methods.

High-resolution nanoLC–tandem mass spectrometry mass spectrometry analysis was performed on a Q Exactive Orbitrap mass spectrometer equipped with an EASY-Spray nano-electrospray ion source (Thermo Fisher Scientific) and coupled to a Thermo Scientific Dionex UltiMate 3000RSLC nano system (Thermo Fisher Scientific). A detailed description and data processing are in Supplementary Material and Methods.

IP-Mass spectrometry

For mass spectrometry analysis, RIP1 was overexpressed using a GFP-tagged vector and immunoprecipitated with GFP-trap_A beads. The data-dependent mass spectra were acquired with the LTQ-Orbitrap mass spectrometer (Thermo Scientific). A detail description of these procedures is in Supplementary Material and Methods.

Results

RIP1 is highly expressed in cancer cells and interacts with HAT1 and SIRT1/2

Programmed necrosis or necroptosis is an alternative form of PCD in which the RIP1–RIP3 complex displays a functional role. To explore RIP1 function in cancer, RIP1 protein levels were evaluated in different cancer cells (Fig. 1A), showing a generally high expression of RIP1. Mass spectrometry analysis performed after RIP1 immunoprecipitation (ProteomeXchange, PRIDE database, dataset identifier PXD007198) identified a new RIP1–HAT1–SIRT1 complex (Fig. 1B). The RIP1–HAT1–SIRT1 complex was validated by Western blot. Both RIP3 (with a weak signal) and HAT4, known interactors of RIP1 and HAT1, respectively (22–24), were found in the complex (Fig. 1C). The fact that both SirT1 and HAT1 immunoprecipitations were reciprocally detecting RIP1 strongly corroborated and strengthened the existence of the RIP1-HAT1-SIRT1 single complex (Supplementary Fig. S1). The observation that both HAT1 and SIRT1 (and 2) were detectable within the RIP1-IP prompted us to investigate whether these acetyltransferases/deacetylases might regulate RIP1 by (de)acetylation. By probing RIP1 immunoprecipitated cells with anti–acetyl-lysine antibody, we observed the presence of an acetylated form of RIP1 (Fig. 1D). Given that RIP1 acetylation has been very debated (25) and never proven in living cells, to investigate the location of RIP1 acetylation sites, high-resolution tandem mass spectrometry was applied. To this end, peptides resulting after digestion with trypsin were separated and analyzed by nano-HPLC coupled to an Orbitrap Q-Exactive mass spectrometer. Data-dependent HCD spectra were obtained on the five most intense mass peaks generated in each scan at resolution of 17,500. Amino acid sequences of high confidence peptides obtained by high-resolution tandem mass spectrometry are reported in Supplementary Figs. S2, S3, and S4 and Supplementary Table S1. Five acetylated lysine residues were identified (Fig. 1E); of these, K115 was localized within the RIP1 kinase domain, whereas K625, K627, K642, and K648 were mapped within the RIP1 DD, suggesting a potential role for acetylation in RIP1 kinase and cell death–regulating functions. Given that RIP1 is localized in the cytoplasm (26), HAT1 and SIRT1 location in the different cellular compartments was studied. Interestingly, although RIP1 confirmed exclusive cytosolic localization, HAT1 and SIRT1 were found in both nuclear and cytosolic compartments, with a higher expression in the cytosol (Fig. 1F).

RIP1 acetylation module is enhanced by SIRT inhibition at sites K596–K599

To assess RIP1, HAT1, and SIRT1/2 relationship, we measured RIP1 acetylation using a newly synthesized pan-SIRT inhibitor, MC2494 (Fig. 2A; Supplementary Table S2 and Supplementary Note), an AGK-2–related molecule (27). This compound displays inhibitory actions against *SIRT1*, *SIRT*, and *SIRT3*/4/5/6, revealing unique features when compared with *SIRT1*- and 2-selective inhibitors (refs. 27–29; Fig. 2B). The IC_{50} values for SIRT1 and 2 inhibition were 38.5 and 58.6 μmol/L,

Figure 4.

The TRAIL–DR5 axis mediates MC2494 cell death. **A,** *TRAIL* and *DR5* expression upon MC2494 (50 μmol/L) for 24 to 30 hours (left), H3K9ac ChIP assay of *DR5*, *TRAIL* promoters followed by qPCR (right). **B,** SIRT1 ChIP assay at *DR5* and *TRAIL* promoters followed by qPCR. **C,** Schematic representation of *TRAIL* promoter and deletion mapping (top). Transient transfection assay reveals that *TRAIL* promoter distal boxes (containing GC-box, AP-1, and ISRE) are essential for activation by MC2494 (bottom). **D,** siRNA silencing of *caspase-8* or *RIP1* and RIP1 pharmacologic inhibition with Necrostatine-1 (Nec-1, 100 μmol/L) abolishes MC2494 apoptosis in U937 cells. **E,** Apoptosis (left) and necrosis (Annexin/PI; right) assays following treatment with MC2494 (50 μmol/L) or vehicle for 24 hours in U937 cells. **F,** Western blot analysis in U937 cells shows a reduction of IAP expression, a no-modulation of CYLD, and an increment of IKKγ protein levels following MC2494 treatment (50 μmol/L and 24 hours). ERKs are loading controls. **G,** Evaluation of RIP1-death impairment in HEK293FT cells transfected with RIP1wt or with the $RIP^{(K596/599R)}$ mutant. **H,** Evaluation of cell death induced by MC2494 in HEK293FT cells transfected with RIP1wt or with the $RIP1^{(K596/599R)}$ mutant. **I,** Protein expression evaluation by Western blot of acetyl lysine (top) and RIP1 (bottom) in HEK293FT cells transfected with RIP1wt and $RIP^{(K596/599R)}$ mutant. Graph showed the mean of three independent experiments with error bars indicating standard deviation.

Published OnlineFirst March 13, 2018; DOI: 10.1158/1078-0432.CCR-17-3081

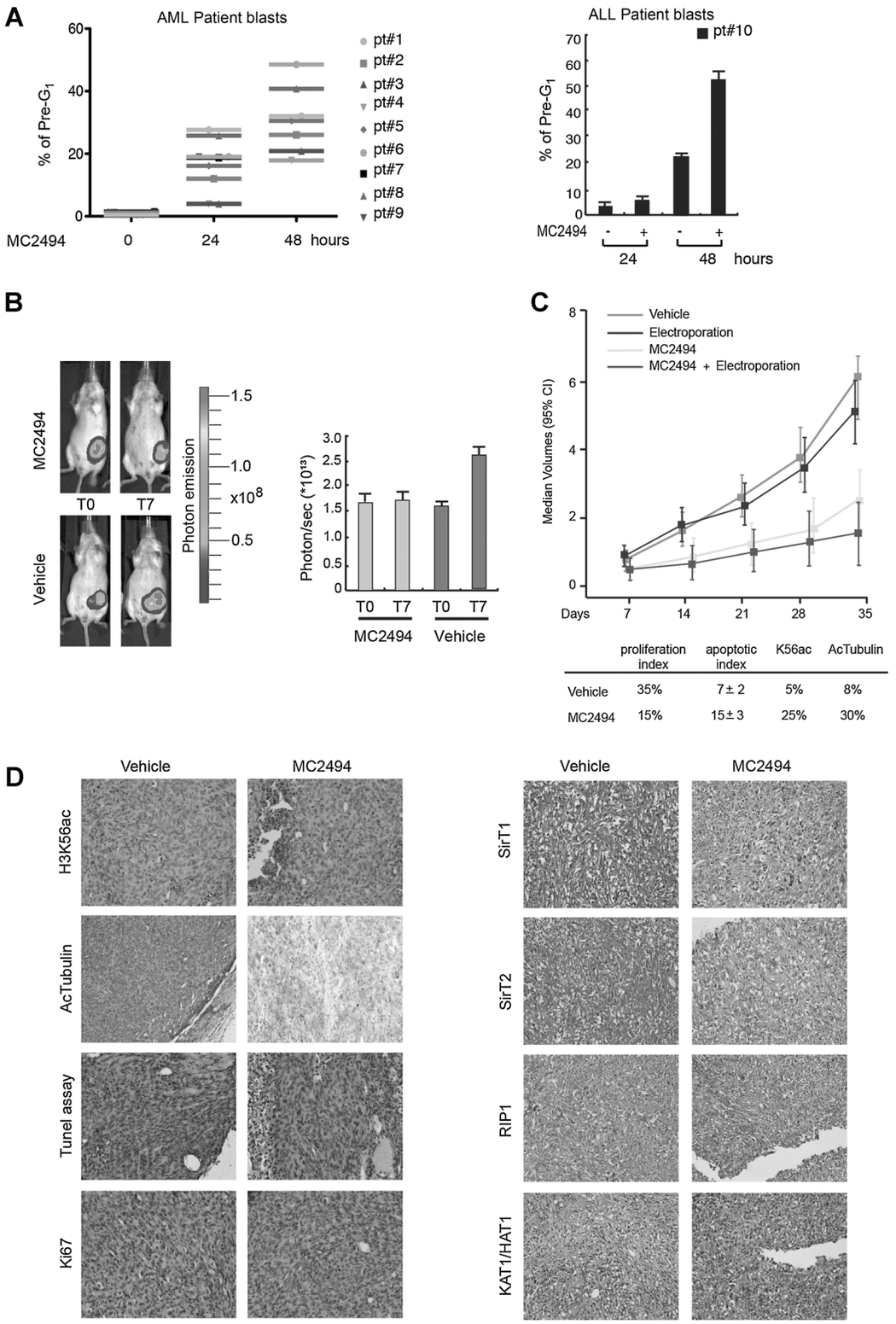

Published OnlineFirst March 13, 2018; DOI: 10.1158/1078-0432.CCR-17-3081

respectively (Supplementary Fig. S5A). Although MC2494-SIRT1 modulation was corroborated on a panel of orthogonal *in vitro* assays (Supplementary Fig. S5B), MC2494 was inactive against both HATs (PCAF) and HDACs (Supplementary Fig. S5C and S5D), suggesting high pan-SIRT specificity. Direct binding between Sirtuins and MC2494 was corroborated by CETSA assay (ref. 30; Supplementary Fig. S5E). Interestingly, although the presence of MC2494 protected SIRTs from thermal degradation, SIRT1/2/3 mRNA and protein levels were reduced in three different cancer systems by MC2494, differently from normal cells (Fig. 2C and D), assuming features of cancer-selectivity. In agreement with the pan inhibitory action, MC2494-induced levels of p53K382 and tubulin acetylation were highly increased, as were H3 (K9-14ac and K56ac) and H4 acetylations (Supplementary Fig. S5F). Excitingly, a strong increase of RIP1 acetylation was observed (Fig. 2E) upon MC2494 stimulation strengthening a possible role of SIRTs in modulating RIP1 (de)acetylation. Mass spectrometry analyses were applied to corroborate these data. Under MC2494 treatment conditions, no qualitative differences were detected in RIP1 acetylation with the exception of the diacetylated peptide 592-603 ($[M+2H]^+$ at m/z 777.88), containing two additional acetylation sites (K596–K599), only detected following MC2494 treatment (Fig. 2F). Interestingly, this region was also identified as the top-score deacetylation site (*P* value: 0.015) by the Predict(S) algorithm of the ASEB web server for lysine acetylation/deacetylation site prediction by selecting the database of 129 known deacetylation sites of SIRT1. Finally, MC2494 regulated the newly identified RIP1 interactome, decreasing SIRT1 expression in the complex, thus unbalancing SIRT1 in favor of HAT1. Also HAT4 and RIP3 were still detectable with a slight increase of RIP3 (Fig. 2G). Interestingly when the HAT inhibitor C646 was used, this drug was able to abrogate RIP1 acetylation, corroborating the involvement of the acetyl transferases in RIP1 acetylation (Supplementary Fig. S6A). This evidence is also supported by the presence of PCAF in the complex (Supplementary Fig. S6B). Moreover, an siRNA approach was performed to corroborate and strengthen these data. Upon *SIRT1* silencing, RIP1 acetylation increased, clarifying the SIRT1-mediated action mechanism of MC2494. (Fig. 2H). These results indicate that RIP1 acetylation at K596–K599 is governed by SIRT inhibition using this novel pan-SIRT inhibitor. To gain more insights into the role of MC2494 in RIP1 acetylation, immunoprecipitation assay was carried out in cells stimulated with one inactive derivative of MC2494, MC2582 (Supplementary Table S2). As expected, MC2582 has no effect on RIP1 acetylation. (Supplementary Fig. S7).

Pan-SIRT inhibition induces caspase-8–dependent cancer-selective cell death

To define the potential biomedical effects of pan-SIRT inhibition and RIP1 complex acetylation, the action of MC2494 was investigated on both leukemia and breast cancer cells. In contrast to EX527 (SIRT1i) and AGK-2 (SIRT2i), MC2494 induced strong proliferation arrest (Fig. 3A; Supplementary Figs. S8 and S9C) and, importantly, did not affect cell cycle or differentiation (Supplementary Fig. S9A and SB). When quantified in real time, MC2494 reduced cell proliferation and migration rate measured by cell index and slope at early time points (Fig. 3B). These data strongly imply wide-ranging antiproliferative effects. Given the hypothesized tumor-selective action, we evaluated the cytotoxic effect of MC2494 by comparing its effect on a broad panel of cancer cells and normal (or immortalized, noncancer) cells. Notably, MC2494 induced cell death in cancer without displaying significant cytotoxicity in normal cells (Fig. 3C). These findings strongly suggest that cell death induction by MC2494 is tumor-specific. Caspase-3/7, -8, -9 activation (Fig. 3D) and dissipation of mitochondrial membrane potential (MMD; Fig. 3E) were induced by MC2494 in cancer cells as was DNA damage measured as increased expression of ATM, ATR, and γH2AX (Fig. 3F). Both players of the extrinsic and intrinsic apoptotic pathways were modulated (Supplementary Fig. S9D and S9E). To gain mechanistic insights, the caspase-8 Z-IETD, caspase-9 Z-LEHD, and pan-caspase Z-VAD inhibitors were tested for their ability to block MC2494 action. Only Z-IETD and Z-VAD completely blocked MC2494-induced PCD, whereas cell death was unaltered in the presence of Z-LEHD, suggesting that caspase-9 activation is dispensable (Fig. 3G). Interestingly, an increment of ROS production occurred upon MC2494 treatment, indicating a possible link between caspase activation, ROS production, and RIP1 expression (Fig. 3H; ref. 31). Therefore, we tested the effect of NAC (32), a known ROS scavenger. Remarkably, in U937 cells, NAC abolished MC2494-induced PCD, demonstrating a causal relevance for ROS production (Fig. 3H).

RIP1 and its acetylation causally activate cancer-selective cell death pathways

To gain insights into PCD mechanism(s), we analyzed the transcriptome of U937 cells treated with MC2494 in comparison with cells treated with the lead SIRT1 inhibitor EX527 (Supplementary Fig. S10A). The 1,245 MC2494 specifically modulated probes were characterized for their relative abundance of Gene Ontology Biological Processes using DAVID (Supplementary Figs. S10B and S11). MC2494 deregulated 116 annotated genes related

Figure 5.

MC2494 displays broad anticancer action *in vitro, ex vivo,* and *in vivo*. **A,** Induction of apoptosis by MC2494 (50 μmol/L) for 24 and 48 hours in 10 *ex vivo* primary AML and ALL blasts. **B,** Representative images of two orthotopic allografted mice with 4T1-luc cells into mammary fat pad. Bioluminescence imaging levels of vehicle- (DMSO) and MC2494-treated mice were acquired at 0 (T0) and after 7 (T7) days of daily treatment and quantified as photon/sec. See Supplementary Table S4 for BLI data in photon/sec. Results are $\sum \pm$ SEM from 7 mice each in the vehicle- and MC2494-treated groups. **C,** MC2494 reduces subcutaneous tumor growth of MDA-MB231 xenograft using s.c. injection of 5×10^6 cells into the left leg of nude mice by and its combination with electrochemotherapy. *In vivo* growth in volume of tumors induced. Two controls (vehicle alone and electroporation of vehicle) are reported to exclude possible effects of the vehicle and electroporation *in vivo*. In the control groups (animals treated with vehicle or electroporation), tumor volumes strongly increased over a 28-day period, whereas MC2494 caused a significant reduction (*P* value 0.005 and 0.001, respectively). An even greater growth inhibition was obtained by the combination of MC2494/electrochemotherapy (*P* value < 0.001) compared with both controls. The weight of all mice assigned to the various groups fell within the same range, providing no immediate evidence for overt toxic effects. Ki67 and TUNEL scores were performed at the end of treatment. The proliferation index was significantly lower in tumors of treated mice compared with controls ($P = 0.002$). Apoptotic index was significantly higher in tumors of MC2494-treated mice ($P = 0.002$). **D,** Immunohistochemical analysis for the apo-index, Ki67, H3K56ac, ac-tubulin, SIRT1, SIRT2, RIP1, and KAT1/HAT1 levels in tumors. Curves and graph presented showed the mean of at least two different experiments with error bars indicating standard deviation.

Published OnlineFirst March 13, 2018; DOI: 10.1158/1078-0432.CCR-17-3081

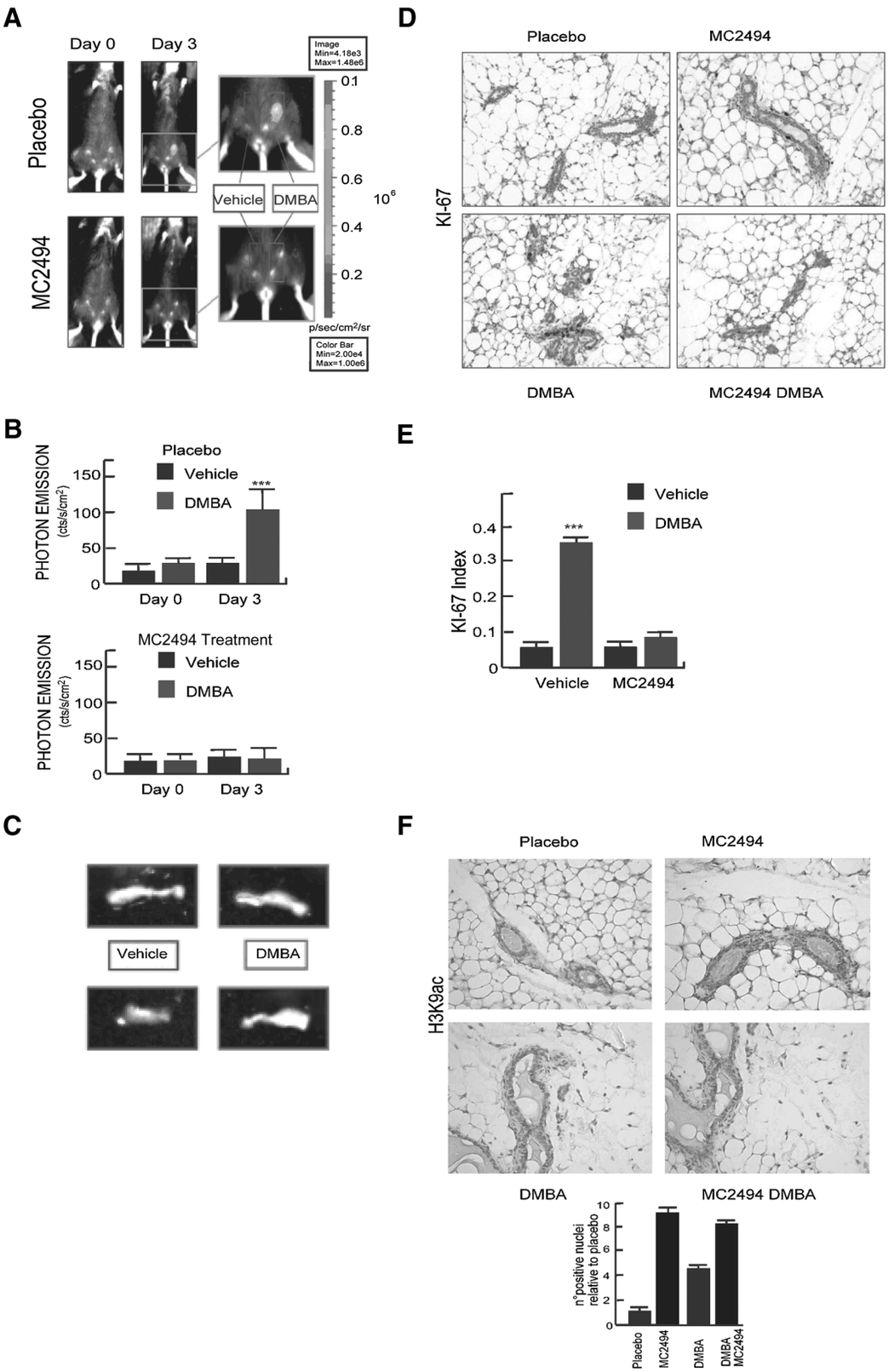

Published OnlineFirst March 13, 2018; DOI: 10.1158/1078-0432.CCR-17-3081

to PCD (FDR = 0.0029), suggesting that this modulation might account for its apoptotic action (or part of it). Strikingly, among the PCD-related targets, *DR5* was selectively upregulated by MC2494 (Supplementary Fig. S10C, $P < 0{,}001$), suggesting that its modulation may account for a potential cancer-selective PCD. Corroborating the transcriptome, PCR confirmed *DR5* induction and supported *TRAIL* mRNA upregulation by MC2494 already after 24 hours of induction. Interestingly, H3ac ChIP followed by qPCR revealed strong acetylation at *TRAIL* and *DR5* promoters after the treatment (Fig. 4A). To elucidate the acetylation modulation at *TRAIL* and *DR5* promoters, SIRT1 ChIP followed by qPCR was performed. Interestingly, SIRT1 occupancy was found at those promoters and was decreased after MC2494 treatment, suggesting an active role for SIRT1 at *TRAIL* and *DR5* promoters (Fig. 4B). We investigated *TRAIL*p by a deletion mapping approach (Fig. 4C). Whereas HDACi selectively targets the proximal GC-box and complexes binding to it (17), MC2494-dependent *TRAIL* activation was strongly reduced by mutations of promoter-distal areas containing the distal GC-box, AP-1, and ISRE. Conversely, mutation of promoter-proximal GC-box led to over 2.5-fold increase, highlighting a potential repressive role of MC2494 on chromatin at this region. Thus, MC2494-driven *TRAIL* activation causally activates the tumor-selective TRAIL/DR5 pathway. To extend the hypothesis that both caspase-8 and RIP1 causally act during MC2494 PCD, we performed loss-of-function experiments in U937 cells. Upon silencing of either *CASP8* or *RIP1*, MC2494-mediated PCD was abolished, suggesting a potentially crucial link between caspase-8 activation and RIP1 function (33) in promoting PCD by MC2494 (Fig. 4C). In support, a similar PCD suppression was observed when pharmacologically blocked RIP1 function after the coadministered with its inhibitor Necrostatine-1 (Nec-1; ref. 34; Fig. 4D). Because RIP1 regulates different types of cell death and survival, we aimed to further distinguish between PCD and necrosis. Data with double Annexin V–propidium iodide (PI) staining strongly indicated that MC2494, like staurosporine, only induced PCD (Fig. 4E). Intriguingly, expression of the E3 ubiquitin ligases IAPs is fully abrogated (ref. 35; Fig. 4E), whereas the expression of IKKγ (NEMO; ref. 36) is induced in the absence of a principal deubiquitinating enzyme, CYLD (refs. 37, 38; Fig. 4F). Collectively, the data suggest a scenario in which, following SIRT inhibition by MC2494 treatment, a PCD pathway is activated, with RIP1 and caspase-8 mediating death and having a causal role. Because RIP1 is acetylated and in the presence of MC2494, the new acetylation occurs at site 596–599 in the RIP1 DD, we applied a mutational approach. Upon transfection in cancer cells, RIP1-mediated cell death was reduced by about 40% with the mutant K596–599R, suggesting that these newly acetylated sites may regulate RIP1 apoptotic function (Fig. 4G). To strength these data, we investigated the effect of MC2494 on $RIP1^{K596-599R}$ (Fig. 4H). Although the point mutation has no impact on the binding between HAT1 and RIP1, cell death induction and RIP1 acetylation undergo a reduction, suggesting the important role of these K residues in driving anticancer activity of MC2494 (Fig. 4I).

MC2494 exerts cancer cell–selective action *ex vivo* and *in vivo*

For primary cancers, acute leukemia blasts were treated *ex vivo* with MC2494 showing a strong increment in pre-G_1 phase (Fig. 5A). MC2494-mediated PCD was clearly detectable at 24 and 48 hours in all 9 primary acute myeloid leukemia (AML) blasts and one acute lymphoid leukemia (ALL) blast, underscoring that in primary cancer, MC2494 induces apoptosis (Fig. 5A; Supplementary Table S3). Pharmacokinetic and *in vitro* half-life studies strengthened a possible use of MC2494 *in vitro* and *in vivo* (Supplementary Fig. S12A–S12D). *In vivo*, MC2494 strongly reduced tumor growth in allograft models as quantified by direct photon emission of luciferase-expressing immunocompetent mice (Fig. 5B; Supplementary Table S4). Moreover, the MDA-MB-231 breast cancer–based xenograft model treated with MC2494 displayed a strong anticancer effect visible as decreased tumor mass. When MC2494 was inoculated by *in vivo* chemoelectroporation, the anticancer effect increased, suggesting its potential *in vivo* also in superficial tumors (as melanoma or other skin tumors in rapid proliferation; Fig. 5C). Following MC2494, apoptosis (tunnel assay), histone and nonhistone SIRT targeting, SIRT1, SIRT2, RIP1, and KAT1/HAT1 were observed in tumors (Fig. 5D), extending results obtained in cell lines.

MC2494 exerts cancer-preventive action *in vivo*

It is a widely shared opinion that cancer prevention is a better approach than treatment. A strategy might include prevention of cancer recurrences and/or action in genetically predisposed patients. Thus, we evaluated the ability of MC2494 to prevent early proliferation occurring in mammary glands after carcinogen exposition. Two groups of MITO-Luc reporter mice (ref. 19; online Methods) were subcutaneously treated with a daily dose of 50 mg/kg MC2494 or placebo (corn oil) for 9 days (9D); at D6, right and left mammary glands were exposed to DMBA or vehicle, respectively. As expected, 3D after DMBA injection in the left mammary gland, bioluminescent emission was detectable in the mice pretreated with placebo (Fig. 6A, placebo). Excitingly, no bioluminescence was detected in the MC2494-pretreated animals, suggesting that the compound was able to fully abrogate DMBA-induced malignant proliferation *in vivo* (Fig. 6A–C). In keeping with these data, Ki-67 proliferation marker was

Figure 6.

MC2494 exerts cancer-preventive effects *in vivo*. **A,** Optical imaging analysis of bioluminescence from MITO-Luc reporter mice injected in the mammary fat pad with DMBA (left) or vehicle (right gland); bioluminescent emission is represented using a pseudo-color scale. Magnified inserts highlight details of photon emission from mammary glands. **B,** Quantitation of **A**. Bars represent average photon emission ± SEM from 4 animals/group measured within the mouse areas shown in the magnified inserts in **A**; bioluminescent emission is completely prevented in MC2494 group as compared with placebo. ***, $P < 0.001$ DMBA ($n = 4$) vs. vehicle-treated ($n = 4$) mammary glands calculated using unpaired *t* test. **C,** *Ex vivo* imaging of mammary glands from two representative mice from each group. **D,** Immunohistochemistry of breast slices obtained from each group stained for Ki67 antibody reveals a marked reduction of cell proliferation in the DMBA + MC2494 as compared with DMBA. **E,** Quantitation of immunohistochemistry in **D**. Bars represent the average ± SEM of the Ki67 index expressed as the ratio between Ki67-positive cells vs. total. ***, $P < 0.001$ DMBA- vs. vehicle-treated mammary glands calculated using two-way ANOVA followed by the Bonferroni *post hoc* test. **F,** Immunohistochemistry and relative quantization of H3K9 acetylation on breast slices obtained from each group; and increased H3K9ac is visible in MC2494-treated animals, corroborating SIRT1/2 inhibition *in vivo*. Graph showed the mean of three independent experiments with error bars indicating standard deviation.

Published OnlineFirst March 13, 2018; DOI: 10.1158/1078-0432.CCR-17-3081

highly expressed in the mammary glands treated with DMBA (Fig. 6D, lower plot, left), but to a much lower extent in glands explanted from MC2494-pretreated mice (Fig. 6D lower plot, right, and Fig. 6E). Increased acetylation of H3K9 in tissues obtained from MC2494-treated mice confirmed that the MC2494 was inhibiting this and likely other epi-targets (Fig. 6F; Supplementary Fig. S11). These experiments suggest that MC2494 counteracts hyperproliferation occurring during the early steps of carcinogenesis, strongly supporting that MC2494 is not only active against an "on-going" cancer, but also acts in a cancer-preventive manner *in vivo*.

Discussion

Our study identifies a new role for Sirtuins and HATs (mainly HAT1; ref. 39) in modulating programmed death pathways. This occurs via a newly identified RIP1–SIRT1/2/HAT1-containing complex and via regulation of RIP1 acetylation. RIP1 (and its acetylation) might represent a key regulatory restriction point between survival, stress, and death. In full agreement, MC2494, a novel pan-SIRT inhibitor (SIRTi; ref. 40), alters the HAT1/SIRT equilibrium in the RIP1 complex. The fact that our MS approach combined with affinity-based chromatography enrichment reveals not only the existence of the RIP1/KAT1/SIRT axes, but also the presence of seven RIP1 acetylation sites (the majority of which are in the DD) adds to a possible regulatory role for acetylation of RIP1-mediated death. In support, mutation of K596–599 to arginine alters RIP1 apoptotic function, suggesting its complex regulation by posttranslational modifications.

The finding that RIP1 is a main player in PCD represents a paradigm shift, identifying (acetylated) RIP1 as an apoptotic player altered in cancer and a potential target of intervention. Based on our findings, we hypothesized that Sirtuins play a key role in restricting RIP1-caspase-8 apoptosis in cancer. The importance of caspase-8 is demonstrated by its causal role, because pharmacologic inhibition and silencing fully block SIRTi-driven death. Pan-SIRT inhibition–mediated anticancer activity is also causally linked to ROS and RIP1, given that treatment with both NAC and Nec-1, and *RIP1* silencing, abolishes PCD. Whether this action also accounts for the tumor-specificity of the pan-SIRTi remains to be established. Evidence that both TRAIL and DR5 are upregulated upon treatment is reminiscent of findings that we (and others; ref. 41) reported for HDACi (17). The contribution of TRAIL tumor-selective PCD by SIRTi is unlikely attributable to HDAC inhibition as MC2494 does not affect the activity of HDACs. Second, cis-acting elements responsible for MC2494 *TRAIL* transcriptional activation are distinct from those reported for HDACi (17). Although our findings strongly suggest that anticancer action of pan-SIRTi can be linked to RIP1 acetylation and TRAIL–DR5 axis activation in cancer (42), the possible tumor-selective activity of pan-SIRTi via TRAIL is a key element because normal cells of diverse origin are all insensitive to pan-SIRT inhibition. Although the role of oxidative stress in TRAIL-mediated apoptosis has been reported (43), our data show that impairment of either caspase-8 or RIP1 fully blocks SIRTi action and that RIP1 acetylation mutant is blandly able to regulate cell death. Possibly, the presence of 7 different RIP1 acetylation sites (only 2 of which are modulated in these settings by SIRTi) suggests that acetylation might control RIP1 cell death functions in a very defined manner. These evidences propose the existence of a caspase-8/RIP1ac-dependent death paradigm of cell death, bound to epigenetic players such as (but not restricted to) Sirtuins and type-B HATs (HAT1; ref. 44). Interestingly, SIRT1 interferes with apoptosis induced by oxidative stress, deacetylating and activating FOXO1 (45), FOXO3a (46), and FOXO4 (47), inducing GADD45 and the mitochondrial antioxidant manganese superoxide dismutase. Each of these factors might contribute to ROS tolerance by SIRT1 alteration in cancer. Deregulation of ROS production, oxidative stress, and FOXO activity are essential steps in cancer development and progression. Moreover, SIRTi induction of apoptosis is accompanied by a marked reduction of IAP and FLICE-inhibitory protein (c-FLIP). Interestingly, IAP reduction (and DR5 activation co-occurrence) was recently reported combining IAP inhibitors with lexatumumab (48). This combination results in apoptosis and vanquish cancer resistance by caspase-8/RIP1ac activation. Thus, new therapeutic regimens may involve SIRTi and remodulation of the RIP1-containing complexes in cancer bypassing resistance to conventional drugs. Consistently, both xenograft and allograft *in vivo* cancer models responded to SIRT inhibition with arrest of progression and disease regression along with increase in apoptotic markers, block of proliferation, SIRT and HAT1 expression resetting, and acetylation within tumors. *Ex vivo* leukemia blasts also undergo PCD upon pan-SIRT inhibition, suggesting a broad range of anticancer actions by MC2494. Though a number of anticancer studies involving SIRTi *in vivo* have been reported (49, 50), to our knowledge, cancer prevention *in vivo* has never been described. The ability of pan-SIRT inhibition to fully prevent chemically induced breast carcinogenesis, concomitantly increasing acetylation *in vivo*, *ex vivo*, and during quantitative measurements, shows its potential use in cancer-preventive settings, which has not been demonstrated before *in vivo*. These preventive features might prove useful in patients who may benefit from a recurrence-preventive approach with low toxicity during follow-up phases and in cases of established cancer predisposition.

Disclosure of Potential Conflicts of Interest

No potential conflicts of interest were disclosed.

Authors' Contributions

Conception and design: V. Carafa, D. Rotili, R. Ragno, A. Mai, L. Altucci
Development of methodology: D. Rotili, G. Citro, A. Chambery, M. Ruvo, P. Ciana, L. Maravigna, E. Radaelli, P. De Antonellis, R. Ragno, A. Mai
Acquisition of data (provided animals, acquired and managed patients, provided facilities, etc.): D. Rotili, A. Baldi, E.P. Spugnini, G. Citro, R. Russo, M. Ruvo, P. Ciana, L. Maravigna, J. Shaik, E. Radaelli, D. Tarantino, M. Zollo, H.G. Stunnenberg
Analysis and interpretation of data (e.g., statistical analysis, biostatistics, computational analysis): V. Carafa, A. Nebbioso, A. Baldi, E.P. Spugnini, G. Citro, A. Chambery, R. Russo, E. Radaelli, R. Ragno, M. Zollo, A. Mai
Writing, review, and/or revision of the manuscript: V. Carafa, D. Rotili, G. Cobellis, M. Ruvo, R. Ragno, A. Mai, L. Altucci
Administrative, technical, or material support (i.e., reporting or organizing data, constructing databases): A. Pirolli
Study supervision: G. Cobellis, M. Zollo, L. Altucci
Other (performed cell-based experiments and was responsible for assembling the figures): F. Cuomo
Other (immunohistochemistry assay and data analysis): P. Bontempo
Other (developing and supervising the chemopreventive assay in reporter mice and testing the activity of the SIRT1 inhibitor): P. Ciana

Acknowledgments

This study was supported by Worldwide Cancer Research (AICR) 15-1002; Blueprint 282510; MIUR20152TE5PK; COST EPICHEMBIO CM1406; EPIGENMIUR-CNR; AIRC-17217; PON_0101227; and Programma VALERE: Vanvitelli per la Ricerca. We thank C. Fisher for linguistic editing and Annamaria Carissimo, Margherita Mutarelli, and Matthias Nees for help in the array analyses and raw data submission.

The costs of publication of this article were defrayed in part by the payment of page charges. This article must therefore be hereby marked *advertisement* in accordance with 18 U.S.C. Section 1734 solely to indicate this fact.

Received October 18, 2017; revised February 20, 2018; accepted March 9, 2018; published first March 16, 2018.

References

1. Galluzzi L, Kroemer G. Secondary necrosis: accidental no more. Trends Cancer 2017;3:1–2.
2. Galluzzi L, Bravo-San Pedro JM, Vitale I, Aaronson SA, Abrams JM, Adam D, et al. Essential versus accessory aspects of cell death: recommendations of the NCCD 2015. Cell Death Differ 2015;22:58–73.
3. Galluzzi L, Baehrecke EH, Ballabio A, Boya P, Bravo-San Pedro JM, Cecconi F, et al. Molecular definitions of autophagy and related processes. EMBO J 2017;36:1811–36.
4. Galluzzi L, Kepp O, Chan FK, Kroemer G. Necroptosis: mechanisms and relevance to disease. Annu Rev Pathol 2017;12:103–30.
5. Vandenabeele P, Galluzzi L, Vanden Berghe T, Kroemer G. Molecular mechanisms of necroptosis: an ordered cellular explosion. Nat Rev Mol Cell Biol 2010;11:700–14.
6. Galluzzi L, Bravo-San Pedro JM, Kroemer G. Necrosis: linking the inflammasome to inflammation. Cell Rep 2015;11:1501–2.
7. Jouan-Lanhouet S, Riquet F, Duprez L, Vanden Berghe T, Takahashi N, Vandenabeele P. Necroptosis, in vivo detection in experimental disease models. Semin Cell Dev Biol 2014;35:2–13.
8. Stanger BZ, Leder P, Lee TH, Kim E, Seed B. RIP: a novel protein containing a death domain that interacts with Fas/APO-1 (CD95) in yeast and causes cell death. Cell 1995;81:513–23.
9. Hsu H, Huang J, Shu HB, Baichwal V, Goeddel DV. TNF-dependent recruitment of the protein kinase RIP to the TNF receptor-1 signaling complex. Immunity 1996;4:387–96.
10. Meylan E, Burns K, Hofmann K, Blancheteau V, Martinon F, Kelliher M, et al. RIP1 is an essential mediator of Toll-like receptor 3-induced NF-kappa B activation. Nat Immunol 2004;5:503–7.
11. Sun L, Wang H, Wang Z, He S, Chen S, Liao D, et al. Mixed lineage kinase domain-like protein mediates necrosis signaling downstream of RIP3 kinase. Cell 2012;148:213–27.
12. Micheau O, Tschopp J. Induction of TNF receptor I-mediated apoptosis via two sequential signaling complexes. Cell 2003;114:181–90.
13. Liu X, Shi F, Li Y, Yu X, Peng S, Li W, et al. Post-translational modifications as key regulators of TNF-induced necroptosis. Cell Death Dis 2016;7:e2293.
14. Festjens N, Vanden Berghe T, Cornelis S, Vandenabeele P. RIP1, a kinase on the crossroads of a cell's decision to live or die. Cell Death Differ 2007;14:400–10.
15. Liu XY, Lai F, Yan XG, Jiang CC, Guo ST, Wang CY, et al. RIP1 kinase is an oncogenic driver in melanoma. Cancer Res 2015;75:1736–48.
16. Lalaoui N, Brumatti G. Relevance of necroptosis in cancer. Immunol Cell Biol 2017;95:137–45.
17. Nebbioso A, Clarke N, Voltz E, Germain E, Ambrosino C, Bontempo P, et al. Tumor-selective action of HDAC inhibitors involves TRAIL induction in acute myeloid leukemia cells. Nat Med 2005;11:77–84.
18. Nebbioso A, Pereira R, Khanwalkar H, Matarese F, Garcia-Rodriguez J, Miceli M, et al. Death receptor pathway activation and increase of ROS production by the triple epigenetic inhibitor UVI5008. Mol Cancer Ther 2011;10:2394–404.
19. Goeman F, Manni I, Artuso S, Ramachandran B, Toietta G, Bossi G, et al. Molecular imaging of nuclear factor-Y transcriptional activity maps proliferation sites in live animals. Mol Biol Cell 2012;23:1467–74.
20. Ciana P, Raviscioni M, Mussi P, Vegeto E, Que I, Parker MG, et al. In vivo imaging of transcriptionally active estrogen receptors. Nat Med 2003;9:82–6.
21. Spano D, Heck C, De Antonellis P, Christofori G, Zollo M. Molecular networks that regulate cancer metastasis. Sem Cancer Biol 2012;22:234–49.
22. Wapenaar H, Dekker FJ. Histone acetyltransferases: challenges in targeting bi-substrate enzymes. Clin Epigenet 2016;8:59.
23. Christofferson DE, Yuan J. Necroptosis as an alternative form of programmed cell death. Curr Opin Cell Biol 2010;22:263–8.
24. Cho YS, Challa S, Moquin D, Genga R, Ray TD, Guildford M, et al. Phosphorylation-driven assembly of the RIP1-RIP3 complex regulates programmed necrosis and virus-induced inflammation. Cell 2009;137:1112–23.
25. Narayan N, Lee IH, Borenstein R, Sun J, Wong R, Tong G, et al. The NAD-dependent deacetylase SIRT2 is required for programmed necrosis. Nature 2012;492:199–204.
26. Wegner KW, Saleh D, Degterev A. Complex pathologic roles of RIPK1 and RIPK3: moving beyond necroptosis. Trends Pharmacol Sci 2017;38:202–25.
27. Outeiro TF, Kontopoulos E, Altmann SM, Kufareva I, Strathearn KE, Amore AM, et al. Sirtuin 2 inhibitors rescue alpha-synuclein-mediated toxicity in models of Parkinson's disease. Science 2007;317:516–9.
28. Trapp J, Meier R, Hongwiset D, Kassack MU, Sippl W, Jung M. Structure-activity studies on suramin analogues as inhibitors of NAD+-dependent histone deacetylases (sirtuins). ChemMedChem 2007;2:1419–31.
29. Napper AD, Hixon J, McDonagh T, Keavey K, Pons JF, Barker J, et al. Discovery of indoles as potent and selective inhibitors of the deacetylase SIRT1. J Med Chem 2005;48:8045–54.
30. Jafari R, Almqvist H, Axelsson H, Ignatushchenko M, Lundback T, Nordlund P, et al. The cellular thermal shift assay for evaluating drug target interactions in cells. Nat Protoc 2014;9:2100–22.
31. Linkermann A, Green DR. Necroptosis. N Engl J Med 2014;370:455–65.
32. Sun SY. N-acetylcysteine, reactive oxygen species and beyond. Cancer Biol Ther 2010;9:109–10.
33. Newton K, Dugger DL, Wickliffe KE, Kapoor N, de Almagro MC, Vucic D, et al. Activity of protein kinase RIPK3 determines whether cells die by necroptosis or apoptosis. Science 2014;343:1357–60.
34. Degterev A, Hitomi J, Germscheid M, Ch'en IL, Korkina O, Teng X, et al. Identification of RIP1 kinase as a specific cellular target of necrostatins. Nat Chem Biol 2008;4:313–21.
35. Bertrand MJ, Milutinovic S, Dickson KM, Ho WC, Boudreault A, Durkin J, et al. cIAP1 and cIAP2 facilitate cancer cell survival by functioning as E3 ligases that promote RIP1 ubiquitination. Mol Cell 2008;30:689–700.
36. Biton S, Ashkenazi A. NEMO and RIP1 control cell fate in response to extensive DNA damage via TNF-alpha feedforward signaling. Cell 2011;145:92–103.
37. O'Donnell MA, Legarda-Addison D, Skountzos P, Yeh WC, Ting AT. Ubiquitination of RIP1 regulates an NF-kappaB-independent cell-death switch in TNF signaling. Curr Biol 2007;17:418–24.
38. O'Donnell MA, Hase H, Legarda D, Ting AT. NEMO inhibits programmed necrosis in an NFkappaB-independent manner by restraining RIP1. PLoS One 2012;7:e41238.
39. Parthun MR.Histone acetyltransferase 1: more than just an enzyme? Biochim Biophys Acta 2013;1819:256–63.
40. Mellini P, Valente S, Mai A. Sirtuin modulators: an updated patent review (2012 - 2014). Expert Opin Ther Pat 2015;25:5–15.
41. Insinga A, Monestiroli S, Ronzoni S, Gelmetti V, Marchesi F, Viale A, et al. Inhibitors of histone deacetylases induce tumor-selective apoptosis through activation of the death receptor pathway. Nat Med 2005;11:71–6.
42. Kim HB, Kim MJ, Lee SH, Lee JW, Bae JH, Kim DW, et al. Amurensin G, a novel SIRT1 inhibitor, sensitizes TRAIL-resistant human leukemic K562 cells to TRAIL-induced apoptosis. Biochem Pharmacol 2012;84:402–10.

Published OnlineFirst March 13, 2018; DOI: 10.1158/1078-0432.CCR-17-3081

43. Lee MW, Park SC, Kim JH, Kim IK, Han KS, Kim KY, et al. The involvement of oxidative stress in tumor necrosis factor (TNF)-related apoptosis-inducing ligand (TRAIL)-induced apoptosis in HeLa cells. Cancer Lett 2002; 182:75–82.
44. Parthun MR.Hat1: the emerging cellular roles of a type B histone acetyltransferase. Oncogene 2007;26:5319–28.
45. Motta MC, Divecha N, Lemieux M, Kamel C, Chen D, Gu W, et al. Mammalian SIRT1 represses forkhead transcription factors. Cell 2004;116: 551–63.
46. Brunet A, Sweeney LB, Sturgill JF, Chua KF, Greer PL, Lin Y, et al. Stress-dependent regulation of FOXO transcription factors by the SIRT1 deacetylase. Science 2004;303:2011–5.
47. van der Horst A, Tertoolen LG, de Vries-Smits LM, Frye RA, Medema RH, Burgering BM. FOXO4 is acetylated upon peroxide stress and deacetylated by the longevity protein hSir2(SIRT1). J Biol Chem 2004;279:28873–9.
48. Basit F, Humphreys R, Fulda S. RIP1 protein-dependent assembly of a cytosolic cell death complex is required for inhibitor of apoptosis (IAP) inhibitor-mediated sensitization to lexatumumab-induced apoptosis. J Biol Chem 2012;287:38767–77.
49. Carafa V, Nebbioso A, Altucci L. Sirtuins and disease: the road ahead. Front Pharmacol 2012;3:4.
50. Carafa V, Rotili D, Forgione M, Cuomo F, Serretiello E, Hailu GS, et al. Sirtuin functions and modulation: from chemistry to the clinic. Clin Epigenetics 2016;8:61.

Published OnlineFirst March 13, 2018; DOI: 10.1158/1078-0432.CCR-17-3081

Clinical Cancer Research

RIP1–HAT1–SIRT Complex Identification and Targeting in Treatment and Prevention of Cancer

Vincenzo Carafa, Angela Nebbioso, Francesca Cuomo, et al.

Clin Cancer Res 2018;24:2886-2900. Published OnlineFirst March 13, 2018.